Reconfigurable Optical Wireless Switches for On-Chip Interconnection

Giovanna Calò, *Member, IEEE*, Loredana Gabriele, Gaetano Bellanca, Jacopo Nanni, *Member, IEEE*, Marina Barbiroli, Franco Fuschini, Velio Tralli, *Senior Member, IEEE*, Davide Bertozzi, *Member, IEEE*, Giovanni Serafino, and Vincenzo Petruzzelli

***Abstract*— Optical Wireless Networks on-Chip have been recently proposed as alternative paradigm to overcome the communication bottleneck in computing architectures based on electrical networks. In this paper, we propose the design of a 3×3 switching matrix for optical wireless on-chip interconnection. The design exploits integrated optical phased arrays to guarantee the communication among three transmitters and three receivers. In this work, the effect of multipath propagation in the on-chip multi-layer structure is taken into account, and the impact of the cladding layer thickness is evaluated. The proposed device is intended to interconnect multiple nodes assuring reconfigurability and high bandwidth.**

***Index Terms*— Wireless optical interconnects, optical antennas, optical phased arrays, on-chip interconnection.**

I. Introduction

NETWORKS on-chip (NoCs), where different cores or processing units are connected through electrical links and switching fabrics [1], are nowadays the most well assessed approach in computing architectures. The constant growth of the computational requirements of data-intensive applications suggests that the performances of conventional electrical NoCs will become limited, since they suffer from scalability bottlenecks, latency-inefficient multi-hop communication and limitations in the delivered communication bandwidth [2]. New solutions for dense system-level integration, such as 3D stacking of 2.5D integration, have been proposed with the aim of reaching bandwidth densities in the order of tera bit per second and high communication power efficiencies that are not achievable with conventional electronics [1], [2].

Different promising solutions, alternative to electrical NoCs, have been proposed in the literature, such as Optical Networks-on-Chip (ONoCs) [3], [4] and Wireless Networks on Chip (WiNoCs) [5], [6], [7].

Optical Networks-on-Chip are based on the integration of an optical layer, housing signal routing and processing components such as switches and filters [8], [9], [10], [11], [12], into computing architectures. The interconnection in the optical domain promises extremely low-latency and bandwidth densities in the order of tens of Tb/s [4].

Different ONoC implementations have been recently proposed for providing optical communication among multiple cores or chiplets stacked on silicon photonic interposers. They mainly exploit Micro Ring Resonator (MRR)-based wired optical interconnections [13], [14], [15], [16]. For example in [16], for modularity and ease-of-integration of different technologies, dedicated electro-optical (E/O) chiplets are introduced as network nodes, taking care of buffering, arbitration, serialization, driving and thermal tuning of both filters and modulators. The basic components of the optical links in these network solutions, i.e., modulators, filters and wavelength division multiplexing (WDM) routing elements, exploit the resonant behavior of MRRs, which need a fine tuning of the resonant wavelengths (e.g. by thermal tuning). Unfortunately, ring tuning results in a significant increase of the overall power budget and is responsible of a remarkable growth of the device complexity, caused by the electrical connections to the ring electrodes. It is also worth mentioning that, in MRR-based networks, an increase in optical parallelism (i.e. number of WDM channels, each one associated to a different wavelength) leads to an impairment of the overall power budget due to the high number of MRRs required.

Another state-of-the-art solution for photonic switching consists of arranging 2×2 Mach-Zehnder Interferometers (MZIs) into higher order switching topologies [17], [18], [19]. Due to their operating principles, MZIs are able to switch multiple wavelengths simultaneously at ns time and without being affected by the data rate carried by individual wavelengths. Such a bandwidth transparency of MZI-based photonic switching elements can be leveraged to adopt dense wavelength-division multiplexed links, reducing the individual data rate per wavelength and increasing signal quality and energy efficiency,

Manuscript received 26 August 2022; revised 1 November 2022; accepted 6 November 2022. Date of publication 24 November 2022; date of current version 24 May 2023. This work was supported in part by the project "IMPACT - Integrated Magneto-biPlAsmonic CirculaTor for any photonic platform" by Apulia region under the call "Progetti di ricerca scientifica innovativi di elevato standard internazionale (art. 22 della legge regionale 30 novembre 2019, n. 52)" and in part by the project "Integrated Magneto-Biplasmonic Circulator For Silicon Platform (IMPACTS)" funded under the call Galileo 2022/ Galilée 2022. *(Corresponding author: Gaetano Bellanca.)*

Giovanna Calò, Loredana Gabriele, and Vincenzo Petruzzelli are with the Department of Electrical Information Engineering, Polytechnic University of Bari, 70125 Bari, Italy (e-mail: giovanna.calo@poliba.it; vincenzo.petruzzelli@poliba.it).

Gaetano Bellanca, Velio Tralli, and Davide Bertozzi are with the Department of Engineering, University of Ferrara, 44122 Ferrara, Italy (e-mail: gaetano.bellanca@unife.it; velio.tralli@unife.it; davide.bertozzi@unife.it).

Jacopo Nanni, Marina Barbiroli, and Franco Fuschini are with the Department of Electrical, Electronic and Information Engineering, University of Bologna, 40136 Bologna, Italy (e-mail: jacopo.nanni3@unibo.it; marina.barbiroli@unibo.it; franco.fuschini@unibo.it).

Giovanni Serafino is with MBI Group, 56121 Pisa, Italy (e-mail: gserafino@mbigroup.it).

Color versions of one or more figures in this article are available at https://doi.org/10.1109/JQE.2022.3224778.

Digital Object Identifier 10.1109/JQE.2022.3224778

while maintaining high aggregate data rates. 2 × 2 MZI switches are typically organized into larger N × N switching topologies through carefully optimized connectivity patterns such as Benes or dilated-Benes networks. For example, in [18] the switch fabric is composed of 56 2 × 2 silicon MZIs, with average on-chip insertion loss of 6.7 dB and 14 dB for the "all-cross" and "all-bar" states, respectively, and useful bandwidth limited to 30 nm.

A recently proposed alternative paradigm, that can compete with ONoCs, is based on Wireless Networks-on-Chip (WiNoCs) [7], [20], [21]. Wireless communication can potentially alleviate the intricacy and overhead of a wired network topology. Moreover, the use of very high frequencies (e.g. mm or THz-waves) in principle allows on-chip integrability, while avoiding inter-router hops and guaranteeing low-latency broadcasting. Miniaturized graphene antennas promise to allow on chip communication in the THz range [22], but the technological challenges to reach such integration are still open.

In this paper, we focus on optical wireless interconnect technology which can enable the implementation of Optical Wireless Networks on-Chip (OWiNoCs), to exploit the best of both wireless and optical communications. Despite pioneering research efforts [23], [24], [25], optical wireless interconnection is still in the early stage of development and its potential is not yet completely explored. However, the feasibility of the approach is supported by the consolidated optical fabrication process and by the demonstrated integrability with CMOS (complementary metal oxide semiconductor) technology.

In [25], we proposed the concept and a first design of an Optical Wireless Switch (OWS) based on transmitting and receiving Optical Phased Arrays (OPA). In this paper, after an initial focus on the architecture of the proposed device, we discuss in detail the characteristics of the antenna element used in these Phased Arrays and then illustrate the radiation patterns as a function of the applied phase shifts, highlighting the variation of the gain in the different configurations. We then report further results obtained by optimizing the design of a 3 × 3 switching matrix. Differently from [25], in this work we exploit the use of five antennas in each OPAs. Moreover, the effect of multipath propagation in the multi-layer on-chip structure is taken into account, and the impact of the cladding layer thickness on the final performance is evaluated. The proposed device is intended to interconnect multiple nodes assuring reconfigurability and high bandwidth, e.g. chiplets in 2.5D manycore systems.

II. On-Chip Wireless Optical Switch

Fig. 1 reports the proposed implementation of a 3 × 3 OWS, in which three input and three output nodes are interconnected through reconfigurable OPAs. The input and output waveguides, together with the OPAs of each communication node, are lying on a dedicated optical layer of the interposer. In the design, Silicon on Insulator (SOI) technology has been considered, but implementations with different approaches are certainly possible.

To maximize the performance of the OWS, each antenna should radiate in parallel M different data channels, thus

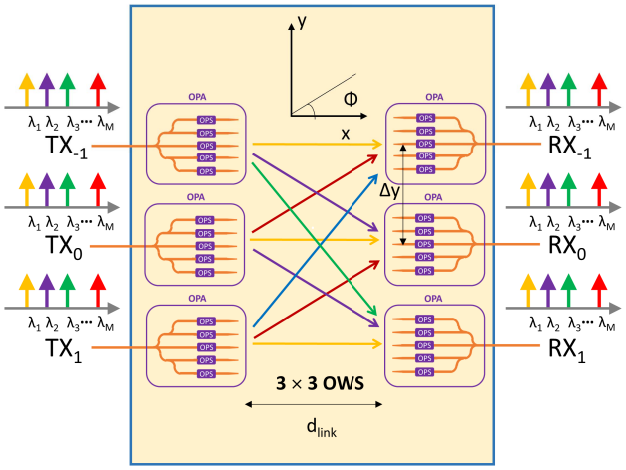

Fig. 1. Scheme of the 3 × 3 on-chip optical wireless switch. OPA: Optical Phase Array; OPS: Optical Phase-Shifter.

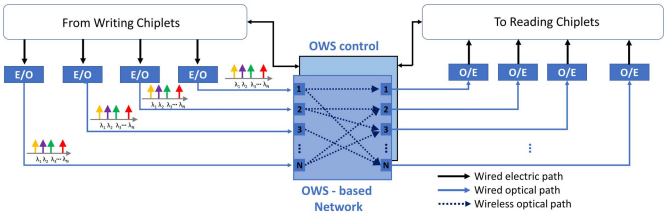

Fig. 2. Scheme of principle of an architecture for inter-core communication based on OWSs. E/O: Electro-optical conversion; O/E: Opto-electrical conversion.

implementing a WDM signal with M wavelengths. Beam steering is obtained by phase-shifting the input signal at each OPA using suitable Optical Phase Shifters (OPSs), therefore allowing the communication with a specific receiver, as schematized by the colored arrows between the transmitters TX_i and the receivers RX_i. To guarantee WDM communications, the needed bandwidth requirements of each component of the OWS (nanoantennas, OPS, couplers and splitters, etc.) should be carefully considered in the design phase.

This OWS is intended to be used as a building block for multi-chiplet wireless interconnection networks, an example of which is shown in Fig. 2. In the conceptual scheme of this figure writing and reading chiplets, acting as network nodes, are connected through electro-optical converters (E/O, i.e., optical transmitters), optical and wireless paths, and opto-electrical converters (O/E, i.e. optical receivers). Fig. 2 also highlights the electronic control logic that is necessary to solve OWS contention when multiple transmitters intend to route optical packets to the same receiver(s). In fact, photonic switching fabrics are intrinsically bufferless, and contention should be managed. The control logic should be designed with the goal to optimize active interposer area and power. The network-level design space exploration is, however, beyond the scope of this paper, which focuses on the OWS design and optimization, and will be the object of future work.

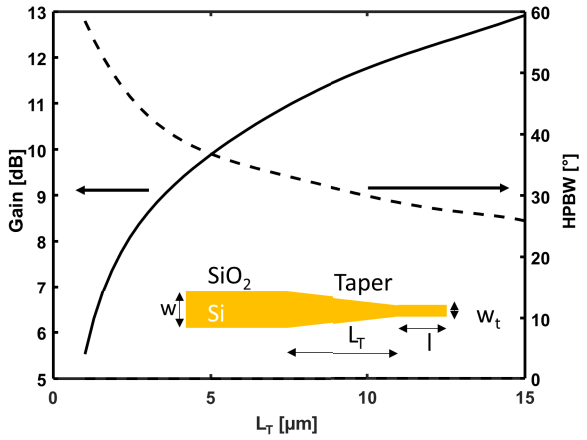

Fig. 3. Maximum gain (solid curve) and Half Power Beam Width (HPBW) (dashed curve) for the taper antenna as a function of the taper length L_T. The scheme of the taper antenna, with the significant geometrical parameters, is shown in the inset. The wavelength is 1550 nm.

III. Design and Optimization of the Antenna Array

A. Radiation Characteristics of the Single Antenna

The proposed 3 × 3 OWS exploits OPAs made by N = 5 taper antennas, both at the transmitters and at the receivers. This configuration with five elements, different with respect to the one proposed in [25], has been chosen as it allows addressing separately all the three nodes of the switch, as detailed below, thus minimizing the crosstalk and maximizing the device performance.

Each node is therefore equipped with 5 taper antennas, schematized in the inset of Fig. 3. The geometry is similar to the one proposed in [23] and obtained by inversely tapering a standard SOI waveguide (cross-section height $h = 220\ nm$ and width $w = 450\ nm$), terminated on a small tip (length $l = 1\ \mu m$, and width $w_T = 130\ nm$). Radiation of the optical signal is taking place along the direction of the mode propagation (x axis of the considered reference system: see Fig. 1). Correct tapering of the structure guarantees excellent impedance matching (back-reflection at the input port of the antenna is less than −35 dB) and suitable radiation properties.

The radiation pattern of this antenna, and its dependence on the geometry of the taper, have been investigated by three-dimensional Finite Difference Time Domain (3D-FDTD) simulations with standard near-to-far field transformation [26]. In these simulations, as required by the near-to-far field projection approach, embedding of the antenna in a homogeneous medium was the considered scenario.

Radiation patterns have been obtained through evaluation of the antenna gain $G(\theta, \varphi)$ by computing the radiation intensity $I(\theta, \varphi)$ in spherical coordinates and in the far-field region, and then normalizing it with respect to the average radiated power on the overall solid angle 4π, according to the definition:

$$G(\theta, \phi) = 4\pi \frac{I(\theta, \phi)}{P_{in}}. \quad (1)$$

Being P_{in} the input power launched into the silicon (Si) waveguide [27], in this evaluation we take into account also the efficiency of the antenna.

The radiated beam can be characterized by considering the maximum gain and the Half Power Beam Width (HPBW), which quantify the capacity of the antenna of focusing the radiated beam in the main radiation direction.

A design parameter, that influences the radiation performances of the taper antenna, is the length of the taper. Figure 3 shows the maximum gain (solid curve) and the HPBW (dashed curve) calculated, for the taper antenna, as a function of the taper length L_T. The HPBW reported in Fig. 3 is defined as the angular separation $\Delta\Phi$, in which the gain decreases by 3 dB. As it can be seen in this figure, the gain increases with the taper length and, accordingly, the radiated beam becomes narrower, as shown by the corresponding decreasing of the HPBW. Indeed, the radiation characteristics of the single antenna influence the radiation performances of the OPA, as it will be described in the following.

B. Radiation Characteristics of the OPA

The OPA configuration analyzed in this paper exploits $N_a = 5$ taper antennas, aligned along the y axis (see Fig. 1). The optical signal in input to each antenna in the OPA can be phase-shifted to steer the radiation beam in the xy plane. The phase shift necessary for the OPA operation can be obtained, in Si waveguides, by using Optical Phase Shifters (OPS) based either on thermo-optic or plasma-optic effect [28].

The radiation diagram of an alignment of N_a identical antennas can be obtained, when they are uncoupled, through multiplication of the electromagnetic field radiated by the single antenna by the corresponding array factor (AF) [27]. To evaluate the array factor, N_a point sources are considered where the antennas of the array are originally positioned, and the total far-field radiated by this array of point sources is analytically calculated. This allows having an easy tool for the design of the array pattern.

The overall radiation diagram of the OPA, in fact, can be suitably designed by choosing the distance d between the antennas in the array. In particular, given a fixed operating wavelength, a single main radiation lobe is obtained when $d \leq \lambda_m$, being λ_m the signal wavelength in the surrounding medium [27]. Conversely, by suitably choosing $d > \lambda_m$, multiple main radiation lobes (i.e. grating lobes) can be exploited to connect the transmitting OPA with the different receivers. This latter approach was adopted in [25] to design 1×5 and 3×3 optical wireless switches based on OPAs with $N_a = 3$ antennas. As anticipated, suitable phase shifts of the input signal to each antenna allow obtaining the desired beam steering.

Differently from [25], in this paper the OPAs exploit $N_a = 5$ antennas with distance $d = \lambda_m$. This choice allows to increase the maximum gain of the OPA and to address 5 different receivers. The 1×5 interconnection is obtained by varying the phase shift α of the excitations of the $N_a = 5$ antennas in the OPA and, consequently, steering of the main lobe in the xy-plane.

As an example, Figs. 4 show the three-dimensional gain radiation diagram of an array of $N_a = 5$ taper antennas, with antenna distance $d = \lambda_m$ and taper length $L_T = 5\ \mu m$, for

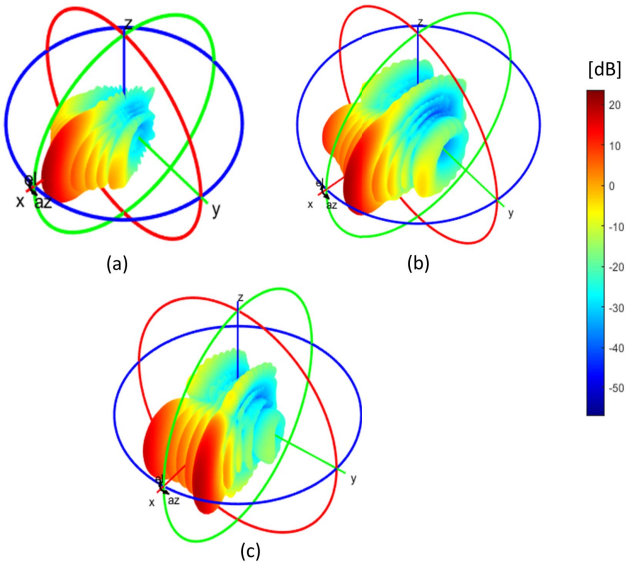

Fig. 4. Three-dimensional gain radiation diagram of an array of N = 5 taper antennas with antenna distance d = λ_m, and taper length $L_T = 5$ μm for the input phase shift values: (a) $\alpha = 0°$, (b) $\alpha = 72°$, and (c) $\alpha = 144°$. The wavelength is 1550 nm.

the input phase shift values: (a) $\alpha = 0°$, (b) $\alpha = 72°$, and (c) $\alpha = 144°$. As shown in Figs. 4 the main radiation beam, directed along the x axis for $\alpha = 0°$, is steered in the xy plane by varying the phase shift α. Moreover, the radiation diagram shows secondary lobes and radiation nulls in the xy plane, i.e the plane identified by the direction x of maximum radiation for the single antenna and the axis y of alignment of the array.

Different receiving nodes can be addressed by steering the main radiation beam. Moreover, to minimize the crosstalk, the main radiation beam should be steered on the same positions of the nulls of the broadside ($\alpha = 0°$) array. The phase shifts necessary to satisfy this requirement can be calculated as $\alpha = \pm p360°/N_a$, with p = 0, 1, 2.

To better describe the array behavior, Figs. 5 show the gain as a function of the angle Φ (measured on the xy plane starting from the x axis – see Fig. 1 as a reference) for different values of the phase shift α calculated for an array of $N_a = 5$ taper antennas with antenna distance d = λ_m, and taper lengths: (a) $L_T = 5$ μm and (b) $L_T = 15$ μm. The gain of the single taper antenna is also reported (black curve).

As shown in Figs. 5, by changing the phase shift of $\alpha = \pm p360°/N_a$, the main radiation lobe is steered in the position of the nulls of the radiation diagram of the broadside array ($\alpha = 0°$). Five different receivers, identified by Rx_i with i = 0, ±1, ±2 in Figs. 5, can be efficiently addressed. The reduction of the maximum gain, that occurs when a phase shift is applied with respect to the case of null phase shift, is due to the radiation diagram of the single taper antenna (black curve in Figs. 5). In fact, the magnitude of the main radiation lobes, for the different values of the phase shift α, follows the envelop of the single antenna radiation diagram. Coherently with the radiation characteristics of the taper antenna shown in Fig. 3, exploiting a longer taper gives higher gain for the OPA (Fig. 5 (b)). At same time, the maximum gain of the steered

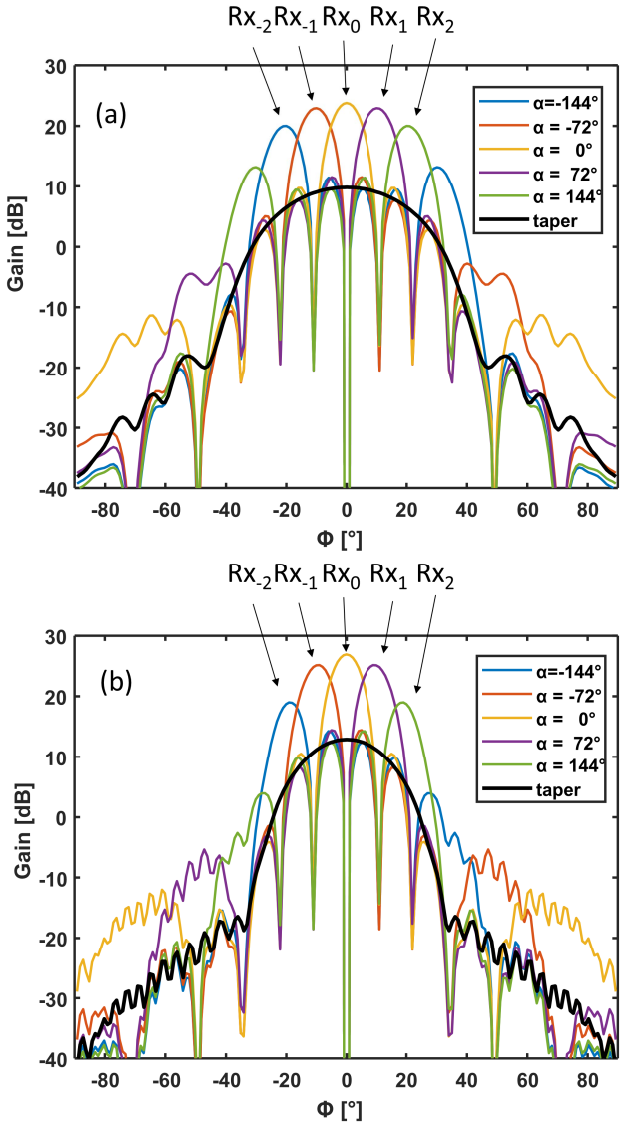

Fig. 5. Gain as a function of the angle Φ for different values of the phase shift α calculated for an array of $N_a = 5$ taper antennas with antenna distance d = λ_m, and taper length is (a) $L_T = 5$ μm and (b) $L_T = 15$ μm. The gain of the taper antenna is also reported (black curve). The wavelength is 1550 nm.

beam varies more significantly with respect to the case of a less directive single antenna (Fig. 5 (a)).

To better quantify this behavior, Fig. 6 shows maximum gain as a function of the taper length $L_T$of an array of $N_a = 5$ taper antennas with antenna distance d= λ_m, for the input phase shift values: $\alpha = 0°$, $\alpha = 72°$, and $\alpha = 144°$.

By increasing the taper length L_T, the difference between the maximum gain at $\alpha = 0°$ and that of the steered beams becomes more pronounced, especially in the case of $\alpha = 144°$ corresponding to the most lateral receiver. Given the proposed application of the OPA for optical wireless switching, it could be advisable to equalize the power received by the different nodes while maximizing the gain of the steered beams. The value of the taper length that compromises well between the aforesaid conditions is $L_T = 5$ μm, and it will be used in the following to simulate the full device.

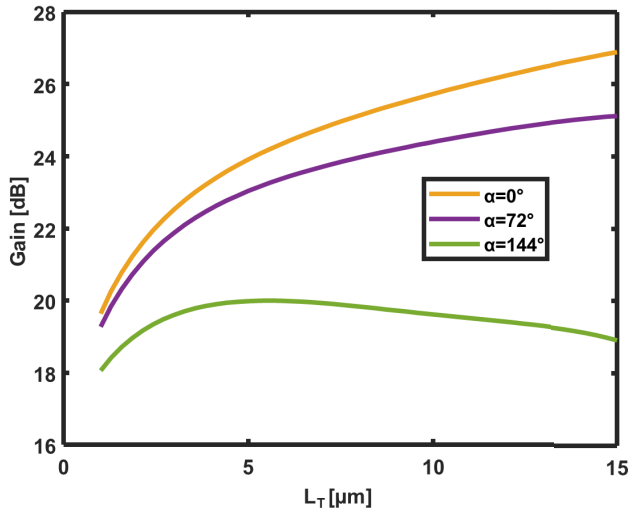

Fig. 6. Maximum gain as a function of the taper length L_T of an array of $N_a = 5$ taper antennas with antenna distance $d = \lambda_m$, for the input phase shift values: $\alpha = 0°$, $\alpha = 72°$, and $\alpha = 144°$. The wavelength is 1550 nm.

The design approach proposed, exploits uncoupled antennas to assess simple design criteria while assuring reconfigurability. In fact, when the antennas are uncoupled, a desired radiation pattern can be synthesized by separately feeding the array elements. The reconfigurability of the OWS is simply achieved by tilting the radiated beam in the propagation plane, through the phase shift of the signal in input to the antennas. The three-dimensional FDTD simulations of the next sections confirm the validity of this simple design approach.

IV. Optimization of the 3 × 3 Optical Wireless Switch

The proposed OPA configuration can address up to five different receivers. These receivers should be placed along the y axis at y = 0 and at the best suited positions given by:

$$y = d_{link} \tan(\Phi_i), \quad (2)$$

where d_{link} is the distance between the transmitter TX_0, and the receiver RX_0, and Φ_i with $i = \pm 1, \pm 2$ is the angular position of the nulls of the radiation diagram obtained with the array in the broadside configuration, i.e. for $\alpha = 0°$.

Actually, the on-chip wireless communication occurs in a multilayered structure, typical of photonic integrated circuits. The medium discontinuities in on-chip optical wireless scenarios, can lead to multi-path propagation phenomena, as shown by the authors in [29]. Multiple reflections cause fluctuations on the received power (increasing where interference is constructive, fading where destructive interference is taking place), requiring simulations of the complete device to optimize the configuration of the OWS.

In particular, here we consider the multilayer structure shown in Fig. 7(a), which corresponds to the sample fabricated and characterized by the authors in [29] for the evaluation of point-to-point wireless links. It consists of a standard SOI sample, where the antennas and the waveguides are patterned, covered by cladding layers that maintain the index

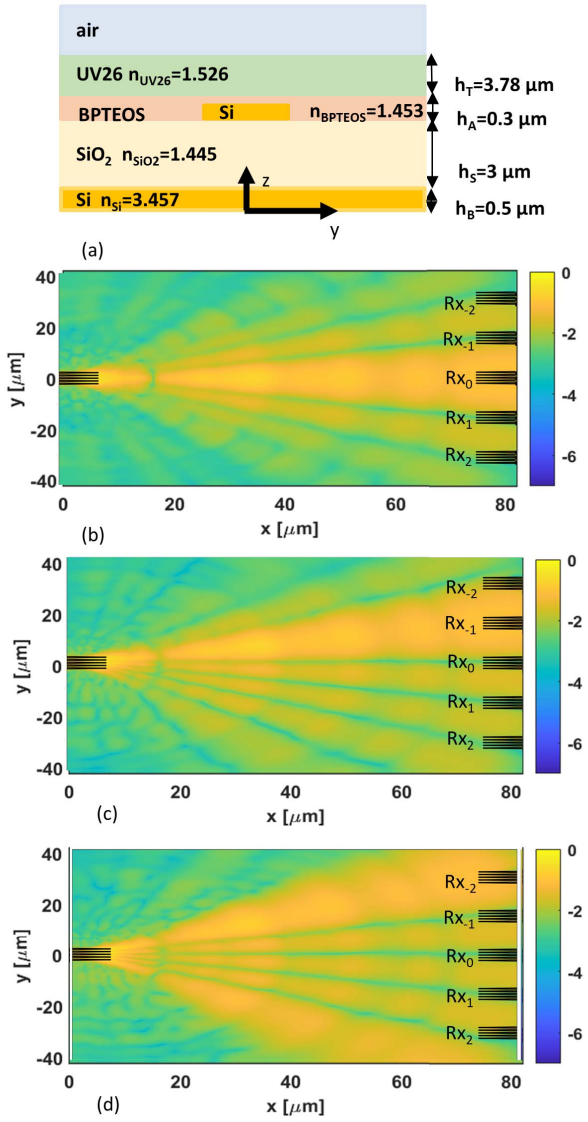

Fig. 7. (a) Scheme of the yz-cross section on-chip multilayered structure. (b-d) 3D-FDTD-simulated electric field pattern (logarithmic scale) in the horizontal plane located in the middle of the waveguide cross-section, for (b) $\alpha = 0°$, (c) $\alpha = 72°$, and (d) $\alpha = 144°$. The solid lines highlight the geometry of the antennas, and the color bar represents the normalized amplitude of the electric field. The wavelength is 1550 nm.

contrast with the silica layer limited. In this way, the radiation diagrams of the antennas are not influenced by close index discontinuities. Both the bottom bulk Si layer and top air layer are considered as semi-infinite, by using Perfectly Matched Layer (PML) boundary conditions.

As shown in Figures 7 (b), (c), and (d), by changing the phase shifts of the input signals applied to the antennas of an OPS, it is possible to address different receivers. When no phase shift is applied (Fig. 7 (b), $\alpha = 0°$) the central transmitter Tx_0 can efficiently address Rx_0. On the contrary, when $\alpha = 72°$ Tx_0 addresses Rx_{-1} (Fig. 7 (c)) whereas the configuration with $\alpha = 144°$ (Fig. 7 (d)) is best suited to address Rx_{-2}.

These figures represent the 3D-FDTD-calculated electric field patterns in the horizontal (xy) plane located in the middle

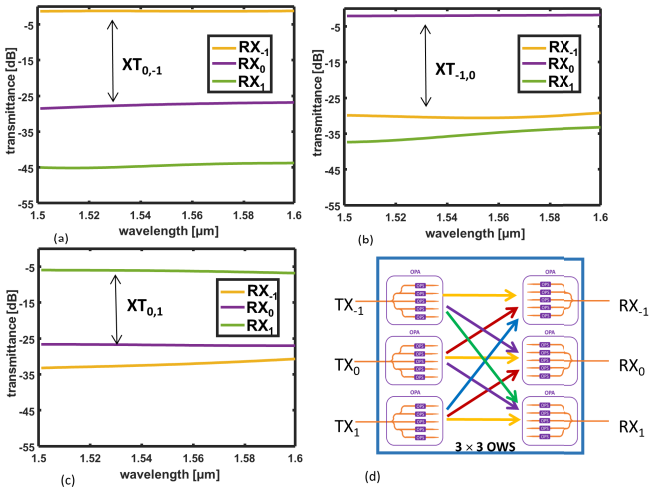

Fig. 8. Transmittance in dB, calculated as a function of the wavelength, at the receiving OPAs, i.e. RX_{+1}, RX_0 and RX_{-1}, when the transmitting OPA TX_{-1} is excited with phase shifts: (a) $\alpha = 0°$, (b) $\alpha = 72°$, and (c) $\alpha = 144°$. The scheme of the 3×3 OWS is also reported in (d). The simulated device exploits reconfigurable OPAs made of 5 taper antennas with taper length $L_T = 5$ μm. The link distance is $d_{link} = 70$ μm. The distance between adjiacent receivers is Δ y = 15.5 μm.

of the antenna layer previously described (plane located in the middle of the waveguide cross-section).

The simulated device exploits reconfigurable OPAs made of 5 taper antennas with taper length $L_T = 5$ μm. The link distance was arbitrarily chosen equal to $d_{link} = 70$ μm.

The field patterns shown in Figs. 7 follow the behavior of the gain radiation diagram in Fig. 5 (a) for the three different phase shift values, but the effect of the propagation in the multilayer is visible since it induces oscillations in the field pattern. However, also in this condition, the direction of the main beam is always maintained.

The same OPA configuration can be exploited to build a 3×3 OWS. In fact, considering the scheme in Fig. 1, a central transmitter node addresses the receiving node RX_0 when the phase shift between the adjacent antennas in the OPA is $\alpha = 0°$. It addresses the receiver RX_{+1} when $\alpha = 72°$, and RX_{-1} when $\alpha = -72°$. A lateral transmitting node, such as TX_1 (or TX_{-1}), illuminates the node RX_1 (or RX_{-1}), positioned in front of it, when $\alpha = 0°$. To address the receiver RX_0 a phase shift of $\alpha = 72°$ ($\alpha = -72°$) is required, whereas a phase shift $\alpha = 144°$ ($\alpha = -144°$) allows to illuminate the receiver RX_{-1} (RX_1).

To guarantee the interconnection between the transmitters and the receivers, it is also necessary to virtually steer the beam of the receiving OPAs in the direction of the maximum incoming radiation, by applying suitable phase shift α at the receiving OPAs.

Given the operation principle of the 3×3 OWS and the symmetry of the device, its behavior can be fully described by considering the link between a lateral transmitter, e. g. TX_{-1}, and the three receivers RX_{-1}, RX_0, and RX_1, schematized in Fig. 1.

As an example, Figs. 8 report the transmittance in dB, calculated as a function of the wavelength, at the receiving OPAs, i.e., RX_{+1}, RX_0 and RX_{-1}, when the transmitting OPA TX_{-1} is excited with phase shifts: (a) α =0°, (b) α =72°, and (c) α =144°.

The scheme of the 3×3 OWS is also recalled in Fig. 8 (d) to ease the reading of the transmittance graphs. As shown in Fig. 8 (a), when the phase shift is $\alpha = 0°$ at the TX_{-1} OPA, the receiver RX_{-1} is connected with an insertion loss about equal to $IL_{-1} \approx -1.3$ dB. The power captured by RX_0 and RX_{+1} is a spurious signal, representing a possible source of crosstalk for the system. The crosstalk can be quantified as:

$$XT_{i,j} = 10Log_{10}\left(\frac{T_{RXi}}{T_{RXj}}\right) \tag{3}$$

where T_{RXj} is the transmittance of the addressed port and T_{RXi} is the transmittance of a non-addressed one. The arrows in Figs. 8 (a)-(c) highlight, for each phase-shift, the curves from which the maximum XT is calculated as the difference in dB between the transmittances. The worst-case insertion loss (i.e., $IL_i = -T_{RXi}$) and crosstalk correspond to the connection between the further nodes TX_{-1} and RX_{+1} (Fig. 8 (c)), as expected from the lower gain of the main lobe in the radiation diagram of Fig. 5 for $\alpha = 144°$ (green curve). In this case, the insertion loss and the crosstalk are, respectively, equal to $IL_1 = 6$ dB and $XT_{0,1} = -21$ dB at the wavelength $\lambda = 1.55$ μm. Coherently with the broadband behavior of the taper antenna [25], the transmittance spectra in Figs 8 do not change significantly with the wavelength. Therefore, the large bandwidth of the device fully covers the C-band.

As mentioned before, in order to guarantee the connection between the transmitter and each of the addressed nodes, a suitable phase shift must be applied also at the receivers (i.e. $\alpha = 0°$, $\alpha = -72°$, and $\alpha = -144°$ for the connections $TX_{-1} \rightarrow RX_{-1}$, $TX_{-1} \rightarrow RX_0$, and $TX_{-1} \rightarrow RX_1$, respectively) to virtually steer the beam of the receiving OPAs in the direction of the maximum radiation. This is feasible by properly phase-shifting the fundamental TE modes in each waveguide at the receiving OPAs.

For a fixed link distance, a parameter that can influence the performance of the OWS is the distance Δy along the y axis between adjacent receivers.

Figures 9 show the transmittance in dB, calculated at the receiving OPAs, i.e. RX_{+1}, RX_0 and RX_{-1}, as a function of the distance Δy between adjacent receivers. The transmitting OPA TX_{-1} is excited with phase shifts: $\alpha = 0°$ (Fig. 9(a)), $\alpha = 72°$ (Fig. 9 (b)), and $\alpha = 144°$ (Fig. 9(c)). Considering Figs. 9 (a) and (b), which correspond to the connections $TX_{-1} \rightarrow RX_{-1}$, $TX_{-1} \rightarrow RX_0$, respectively, the performances of the OWS in terms of insertion loss do not change significantly with Δy. Moreover, in both cases, the crosstalk remains below -20 dB.

Considering the link between the transmitter and the furthermost receiver $TX_{-1} \rightarrow RX_1$(Fig. 9 (c)), the transmittance (green curve) is maximized, i.e., the insertion loss is minimized, when $\Delta y = 15.5$ μm. The Δy value, obtained by the 3D-FDTD parametric analysis of the full device, is very near to the one $\Delta y \approx 15$ μm evaluated through Eq. 2. Therefore, Eq. 2 gives a good estimation of the receiver positions. Also from the point of view of the crosstalk, the distance

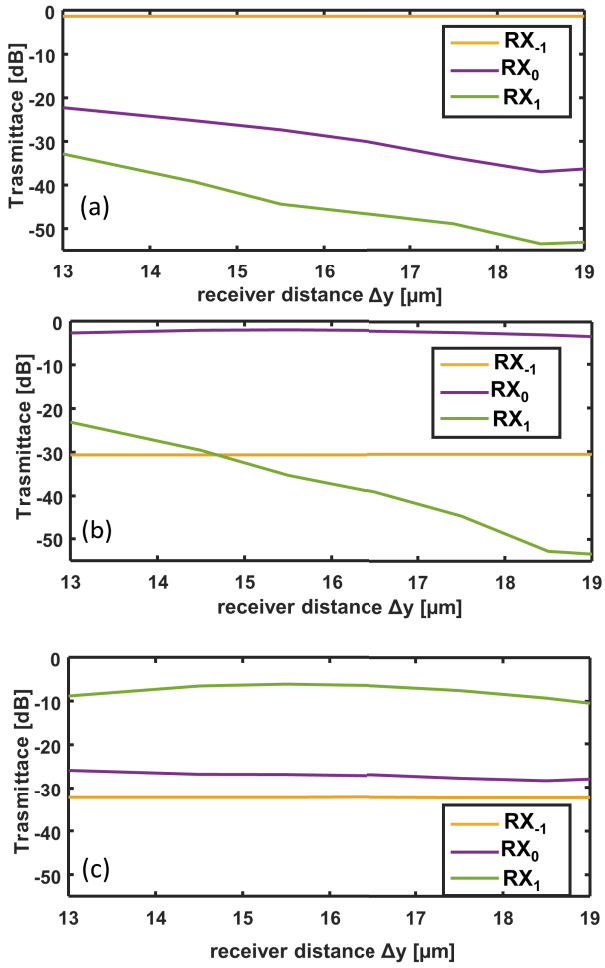

Fig. 9. Transmittance in dB, calculated at the receiving OPAs, i.e. RX_{+1}, RX_0 and RX_{-1}, as a function of the distance Δy between adjacent receivers. The transmitting OPA TX_{-1} is excited with phase shifts: (a) $\alpha = 0°$, (b) $\alpha = 72°$, and (c) $\alpha = 144°$. The simulated device exploits reconfigurable OPAs made of 5 taper antennas with taper length $L_T = 5$ μm. The link distance is $d_{link} = 70$ μm and the wavelength is $\lambda = 1.55$ μm.

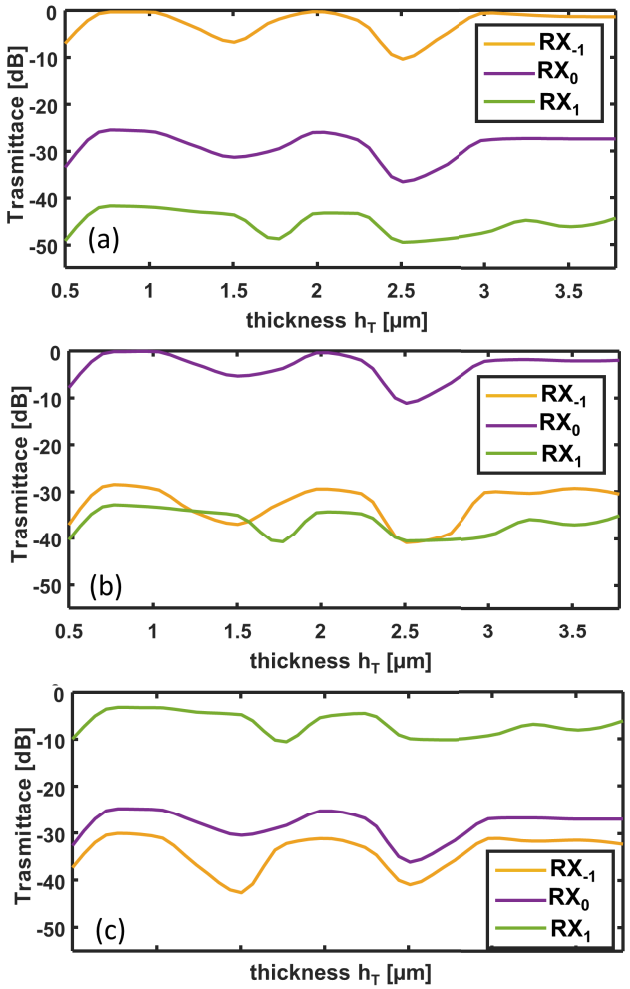

Fig. 10. Transmittance in dB, calculated at the receiving OPAs, i.e. RX_{+1}, RX_0 and RX_{-1}, as a function of the cladding thickness h_T. The transmitting OPA TX_{-1} is excited with phase shifts: (a) $\alpha = 0°$, (b) $\alpha = 72°$, and (c) $\alpha = 144°$. The simulated device exploits reconfigurable OPAs made of 5 taper antennas with taper length $L_T = 5$ μm. The link distance is $d_{link} = 70$ μm, the distance between adjacent receivers is $\Delta y = 15.5$ μm, and the wavelength is $\lambda = 1.55$ μm.

$\Delta y = 15.5$ μm optimizes the performances when the further receiver RX_1 is addressed.

As analyzed in [29] for point-to-point links between single antennas, the behavior of the electromagnetic propagation in a multilayered medium depends on the layer characteristics. Here, we investigate the effect of the variation of the cladding layer thickness (UV26 layer), which is a deposited polymer used to increase the distance between the radiator and the interface with the air. The constructive or destructive interference, caused by the phenomenon of multiple reflections and transmissions at the interfaces, is sensitive to the layer thickness variation. The layer thickness can be, therefore, considered as a degree of freedom available for engineering the propagation channel and for improving the link performances.

Figures 10 show the transmittance in dB, calculated at the receiving OPAs, i.e. RX_{+1}, RX_0 and RX_{-1}, as a function of the cladding thickness h_T. Also in this case, the transmitting OPA TX_{-1} is excited with phase shifts: (a) $\alpha = 0°$, (b) $\alpha = 72°$, and (c) $\alpha = 144°$. The variation of the cladding layer thickness h_T, for a fixed link distance $d_{link} = 70$ μm, induces oscillations of the transmittance curves at the three analyzed receivers.

In order to verify the performances of the OWS in the whole considered wavelength range, Figs. 11 (a), (b), and (c) report the insertion loss as a function of the wavelength and of the cladding thickness h_T calculated at the addressed receivers: (a) Rx_{-1} for the connection $TX_{-1} \rightarrow RX_{-1}$, (b) Rx_0 for the connection $TX_{-1} \rightarrow RX_0$, and (c) Rx_{+1} for the connection $TX_{-1} \rightarrow RX_1$.

As it can be seen from Figs. 11, for a fixed value of the layer thickness h_T, the insertion loss is almost constant, with a maximum variation of less than 3 dB.

Similarly, Figs. 11 (d), (e), and (f) show the worst-case crosstalk (calculated according to eq. 3) as a function of the cladding thickness h_T and of the wavelength: (d) $XT_{0,-1}$ for the connection $TX_{-1} \rightarrow RX_{-1}$, (e) $XT_{-1,0}$ for the connection $TX_{-1} \rightarrow RX_0$, and (f) $XT_{0,1}$ for the connection $TX_{-1} \rightarrow RX_1$.

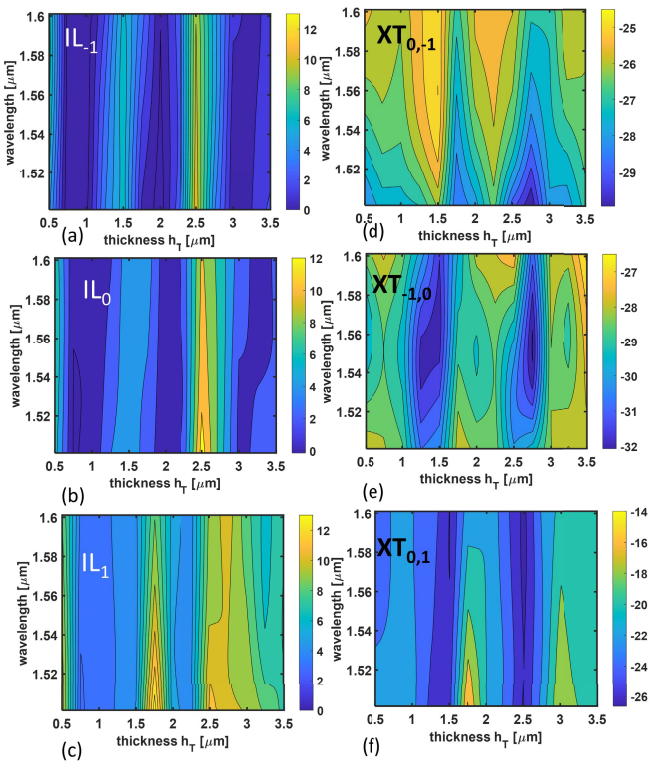

Fig. 11. (a-c) Insertion loss as a function of the wavelength and of the cladding thickness hT: (a) IL_{-1} for the connection $TX_{-1} \rightarrow RX_{-1}$, (b) IL_0 for the connection $TX_{-1} \rightarrow RX_0$, and (c) IL_{+1} for the connection $TX_{-1} \rightarrow RX_1$. (d-f) Worst case crosstalk as a function of the cladding thickness hT and of the wavelength: (d) $XT_{0,-1}$ for the connection $TX_{-1} \rightarrow RX_{-1}$, (e) $XT_{-1,0}$ for the connection $TX_{-1} \rightarrow RX_0$, and (f) $XT_{0,1}$ for the connection $TX_{-1} \rightarrow RX_1$.

For a fixed value of the cladding thickness, the variation of the crosstalk with the wavelength is more pronounced than that of the insertion loss, but the crosstalk remains in general well below -14 dB, with a maximum variation with the wavelength of 7 dB.

Considering Figs. 10 and 11, the cladding layer thickness that maximizes the transmittance at the further receiver, which is the most critical one, is $h_T = 1$ μm. In this case the worst-case insertion loss is equal to $IL_1 = 3$ dB, and the crosstalk is -21 dB.

The fabrication of the proposed OWS requires the design of the network feeding the antennas in the OPA and of the phase shifters. A possible implementation of the feeding network that brings the signal to the OPA antennas can be made by cascading multiple beam splitters. For example, 1×2 Y junctions can be cascaded to increase the number of outputs, starting from a single input waveguide. A 1×2 Y junction keeps the two outputs in phase, while equally dividing the input power into the two waveguides. Another possible implementation of a 1×2 beam splitter can be made by using multi-mode interference (MMI) devices. Both 1×2 Y beam splitter and 1×2 MMI exhibit a broadband behavior and are not expected to significantly alter the OWS bandwidth.

More elaborated solutions can also be implemented such as $1 \times N$ MMIs, following the design criteria reported in reference [30]. In this case, the beam can be split into multiple outputs in a single stage. The phase shift between the outputs of the $1 \times N$ MMI, and eventual additional phase shifts coming from different lengths of the optical paths, can be compensated by a calibration of the phase tuning.

Phase shifters can be implemented exploiting either plasma-optic or thermo-optic effect. Thermally controlled waveguide phase shifters could be preferred because they are based on relatively simple and robust structures and their fabrication is less prone to errors. These phase actuators need to be calibrated and thermal crosstalk must be taken into account in the design of the circuit. To overcome this issue, an approach to cancel out the effects of the phase coupling induced by thermal crosstalk in photonic integrated circuits, with thermal phase actuators, can be applied [31].

A further issue related to fabrication is the tolerance to fabrication errors. The most significant error that can affect the behavior of the OWS is a variation Δd of the antenna distance in the OPAs. A change in the distance between the antennas due to fabrication errors can cause a change of the beam shape of the OPA radiation diagram. In particular, we verified that the zeros of the radiation diagram shift of less than 2° when $0 < \Delta d < 100$ nm. In order to verify if the change of the shape of the radiated beam can cause an effect on the insertion loss and on the crosstalk, it is necessary to simulate the overall device, considering the propagation in the multilayer structure and the physical size of the OPAs. For this purpose, we simulated the overall OWS for different values of the distance between the antennas in the OPAs. In all the simulations, the receivers were placed along the y axis in the optimal design positions, i.e. with distance $\Delta y = 15.5$ μm between adjacent receivers. By this parametric analysis, we verified that a change of $\Delta d = 100$ nm of the antenna distance causes a maximum variation of the insertion loss lower than 2 dB. This is due to the variation of the beam shape and of the multipath contribution and it occurs, in particular, when the further receiver R_{x-1} is addressed. In all the considered cases, the worst-case crosstalk remained below -18 dB.

V. Conclusion

The design of a 3×3 optical wireless router allowing on-chip optical wireless interconnections has been proposed and discussed. The OWS exploits reconfigurable OPAs made of five taper antennas with taper length $L_T = 5$ μm, either at the transmitting and at the receiving nodes. The antennas in the arrays are aligned along the y axis with distance equal to the wavelength in the propagation medium ($d = \lambda_m$). The interconnection among the different nodes is obtained by steering the beam of the transmitting and receiving antennas, through the variation of the phase difference between the elements of the arrays. The proposed configuration improves the connection performances with respect to the one reported in [25] in terms of crosstalk and insertion loss of about 4 dB and 10 dB, respectively, to parity of multilayer structure. This improvement is mainly due to the design choice of using $N_a = 5$ antennas with distance $d = \lambda_m$ in the OPAs, which

increase the maximum gain of the antennas and avoid the use of grating lobes for communication.

A further degree of freedom, investigated to optimize the device, is the thickness of the cladding layer which influences the multi-path propagation. A minimum value of the worst-case insertion loss $IL_1 = 3$ dB is achieved, thus improving the device performances of further 3 dB.

An interesting feature of the proposed OWS is the large bandwidth, with respect to MRR resonators or MZIs switches. For example, if a WDM signal is used for communication, with channel spacing $\Delta\lambda = 0.8$ nm virtually about 120 channels can be allocated in the simulated 100-nm bandwidth of the OWS. Given the broadband behavior, all the allocated WDM channels can be switched at the same time, thus making the power requirement for signal routing independent from the number of WDM channels. Consequently, the required energy-per-bit, given by the power over the aggregated bit rate (i.e. bit rate per channel multiplied by the number of WDM channels), decreases with the number of WDM channels. Even though a direct comparison of performances is not straightforward, the proposed OWS can be a promising alternative to MRR- and to MZI-based networks. Thanks to its broadband operation, it can allow WDM schemes, as in MZI networks. Moreover, thanks to its non-resonant behavior, it does not require an extremely fine tuning as in MRR networks.

REFERENCES

[1] J. Flich and D. Bertozzi, *Designing Network-on-Chip Architectures in the Nanoscale Era*. Boca Raton, FL, USA: CRC Press, 2019.

[2] G. P. Nychis, C. Fallin, T. Moscibroda, O. Mutlu, and S. Seshan, "On-chip networks from a networking perspective: Congestion and scalabilityin many-core interconnects," *ACM SIGCOMM Comput. Commun. Rev.*, vol. 42, no. 4, pp. 407–418, 2012.

[3] M. Zia, C. Wan, Y. Zhang, and M. Bakir, "Electrical and photonic off-chip interconnection and system integration," in *Optical Interconnects for Data Centers*. Amsterdam, The Netherlands: Woodhead Publishing, 2017, pp. 265–286.

[4] N. Terzenidis et al., "Board- and rack-scale optical interconnection architectures for disaggregated data centers," *Proc. SPIE*, vol. 11286, Feb. 2020, Art. no. 1128606.

[5] S. Deb and H. Mondal, "Wireless network-on-chip: A new era in multi-core chip design," in *Proc. 25th IEEE Int. Symp. Rapid Syst. Prototyping*, Oct. 2014, pp. 59–64.

[6] X. Timoneda et al., "Engineer the channel and adapt to it: Enabling wireless intra-chip communication," *IEEE Trans. Commun.*, vol. 68, no. 5, pp. 3247–3258, May 2020.

[7] S. Abadal, A. Mestres, J. Torrellas, E. Alarcon, and A. Cabellos-Aparicio, "Medium access control in wireless network-on-chip: A context analysis," *IEEE Commun. Mag.*, vol. 56, no. 6, pp. 172–178, Jun. 2018.

[8] A. Shacham, K. Bergman, and L. P. Carloni, "On the design of a photonic network-on-chip," in *Proc. 1st Int. Symp. Netw.-on-Chip (NOCS)*, May 2007, pp. 53–64.

[9] A. Kazmierczak et al., "Highly integrated optical 4×4 crossbar in silicon-on-insulator technology," *J. Lightw. Technol.*, vol. 27, no. 6, pp. 3317–3323, Aug. 1, 2009.

[10] G. Calò, D. Alexandropoulos, A. D'Orazio, and V. Petruzzelli, "Wavelength selective switching in dilute nitrides multi quantum well photonic band gap waveguides," *Phys. Status Solidi B*, vol. 248, no. 5, pp. 1212–1215, May 2011.

[11] S. Abadian, G. Magno, V. Yam, and B. Dagens, "Broad-band plasmonic isolator compatible with low-gyrotropy magneto-optical material," *Opt. Exp.*, vol. 29, no. 3, pp. 4091–4104, 2021.

[12] G. Calò, A. Farinola, and V. Petruzzelli, "Equalization in photonic bandgap multiwavelength filters by the Newton binomial distribution," *J. Opt. Soc. Amer. B, Opt. Phys.*, vol. 28, no. 7, pp. 1668–1679, 2011.

[13] N. Sherwood-Droz et al., "Optical 4×4 hitless silicon router for optical networks-on-chip (NoC)," *Opt. Exp.*, vol. 16, no. 20, pp. 15915–15922, 2008.

[14] Q. Cheng, M. Bahadori, Y.-H. Hung, Y. Huang, N. Abrams, and K. Bergman, "Scalable microring-based silicon clos switch fabric with switch-and-select stages," *IEEE J. Sel. Topics Quantum Electron.*, vol. 25, no. 5, pp. 1–11, Sep. 2019.

[15] M. Tala, O. Schrape, M. Krstic, and D. Bertozzi, "Interfacing 3D-stacked electronic and optical NoCs with mixed CMOS-ECL bridges: A realistic preliminary assessment," in *Proc. Great Lakes Symp. VLSI*, May 2018, pp. 81–86.

[16] Y. Thonnart, S. Bernabe, J. Charbonnier, C. Bernard, D. Coriat, and C. Fuguet, "POPSTAR: A robust modular optical NoC architecture for chiplet-based 3D integrated systems," in *Proc. Design, Autom. Test Eur. Conf. Exhib. (DATE)*, Mar. 2020, pp. 1456–1461.

[17] L. Lu, L. Zhou, Z. Li, X. Li, and J. Chen, "Broadband 4×4 non-blocking silicon electrooptic switches based on Mach–Zehnder interferometers," *IEEE Photon. J.*, vol. 7, no. 1, pp. 1–8, Feb. 2015, doi: 10.1109/JPHOT.2015.2390195.

[18] L. Lu et al., "16×16 non-blocking silicon optical switch based on electro-optic Mach–Zehnder interferometers," *Opt. Exp.*, vol. 24, pp. 9295–9307, May 2016.

[19] G. Calo and V. Petruzzelli, "WDM performances of two- and three-waveguide Mach–Zehnder Switches assembled into 4×4 matrix router," *Prog. Electromagn. Res. Lett.*, vol. 38, pp. 1–16, 2003.

[20] F. Lemic et al., "Survey on terahertz nanocommunication and networking: A top-down perspective," *IEEE J. Sel. Areas Commun.*, vol. 39, no. 6, pp. 1506–1543, Apr. 2021.

[21] M. F. Imani, S. Abadal, and P. del Hougne, "Metasurface-programmable wireless network-on-chip," *Adv. Sci.*, vol. 9, no. 26, Sep. 2022, Art. no. 2201458.

[22] S. Abadal, S. E. Hosseininejad, A. Cabellos-Aparicio, and E. Alarcon, "Graphene-based terahertz antennas for area-constrained applications," in *Proc. 40th Int. Conf. Telecommun. Signal Process. (TSP)*, Barcelona, Spain, Jul. 2017, pp. 817–820.

[23] C. García-Meca et al., "On-chip wireless silicon photonics: From reconfigurable interconnects to lab-on-chip devices," *Light, Sci. Appl.*, vol. 6, no. 9, Sep. 2017, Art. no. e17053.

[24] F. Fuschini et al., "Multi-level analysis of on-chip optical wireless links," *Appl. Sci.*, vol. 10, no. 1, p. 196, 2020.

[25] G. Calò et al., "Design of reconfigurable on-chip wireless interconnections through optical phased arrays," *Opt. Exp.*, vol. 29, pp. 31212–31228, Sep. 2021.

[26] *Lumerical Solutions*. Accessed: Dec. 15, 2022. [Online]. Available: https://www.ansys.com/products/photonics

[27] R. E. Collin, *Antennas and Radiowave Propagation*. New York, NY, USA: McGraw-Hill, 1985.

[28] W. N. Ye and Y. Xiong, "Review of silicon photonics: History and recent advances," *J. Modern Opt.*, vol. 60, no. 16, pp. 1299–1320, Sep. 2013.

[29] J. Nanni et al., "Multi-path propagation in on-chip optical wireless links," IEEE Photonics Technol. Lett. vol. 32, no. 17, pp. 1101–1104, 2020.

[30] L. B. Soldano and E. C. M. Pennings, "Optical multi-mode interference devices based on self-imaging: Principles and applications," *J. Lightw. Technol.*, vol. 13, no. 4, pp. 615–627, Apr. 15, 1995.

[31] M. Milanizadeh, D. Aguiar, A. Melloni, and F. Morichetti, "Canceling thermal cross-talk effects in photonic integrated circuits," *J. Lightw. Technol.*, vol. 37, no. 4, pp. 1325–1332, Feb. 15, 2019.

Giovanna Calò (Member, IEEE) received the master's degree in electronic engineering and the Ph.D. degree in electromagnetism from the Polytechnic University of Bari, Bari, Italy, in 2002 and 2006, respectively.

She joined the Department of Electrical and Electronic Engineering, Polytechnic University of Bari, in 2002, where she is currently an Associate Professor of electromagnetism. Her main research interests are computational electromagnetics, on-chip optical interconnections, integrated plasmonic nanoantennas for wireless on-chip optical communications, photonic crystals, and plasmonic nanostructures and components.

Loredana Gabriele received the bachelor's degree in electronic and telecommunication engineering from the Polytechnic University of Bari, Bari, Italy, in 2021, where she is currently pursuing the master's degree in telecommunication engineering. Her main research interests include on-chip wireless communication and integrated nanoantennas.

Gaetano Bellanca received the M.Sc. degree in electronic engineering and the Ph.D. degree in electronic and computer science from the University of Bologna, in 1991 and 1995, respectively. He joined the Department of Engineering, University of Ferrara, in 1999, where he is currently an Associate Professor of electromagnetics. His main research interests are in the design and characterization of optical components and devices, development of numerical techniques for electromagnetics in the fields of applied microwave, and antennas and integrated optics.

Jacopo Nanni (Member, IEEE) received the B.Sc. and M.Sc. degrees in telecommunications engineering from the University of Bologna, Italy, in October 2012 and March 2015, respectively, and the double Ph.D. degrees from the University of Bologna and Université Paris-Est, ESYCOM, ESIEE Paris, Noisy-le-Grand (France), in December 2018, working on low cost and low consumption radio-over-fiber (RoF) systems based on vertical cavity surface emitting lasers (VCSELs) for indoor applications. In July 2021, he Joined the Department of Electrical, Electronic and Information Engineering "Guglielmo Marconi," University of Bologna, as a Research Associate. He is currently working on RoF systems for efficient cellular network infrastructures and in the field of radioastronomy within the Square Kilometer Array (SKA) Project. Moreover, a part of his work was dedicated to the study of optical wireless networks on-chip and the optimization of low-cost optical coupling structures.

Marina Barbiroli received the Laurea degree in electronic engineering and the Ph.D. degree in computer science and electronic engineering from the University of Bologna, in 1995 and 2000, respectively.

Since 2020, she has been an Associate Professor at Bologna University. Her research interests are on propagation models for mobile communications systems, with focus on wideband channel modeling for 5G systems, investigation of planning strategies for mobile systems, broadcast systems and broadband wireless access systems, analysis of exposure levels generates by all wireless systems, and for increasing spectrum efficiency. The research activity includes the participation to European research and cooperation programs (COST 259, COST 273 COST2100, COST IC004, and COST IRACON) and in the European Networks of Excellence FP6-NEWCOM and FP7-NEWCOM++.

Franco Fuschini received the M.Sc. degree in telecommunication engineering and the Ph.D. degree in electronics and computer science from the University of Bologna, in March 1999 and July 2003, respectively. He is currently an Associate Professor with the Department of Electrical, Electronic and Information Engineering "G. Marconi," University of Bologna. He is the author or the coauthor of more than 30 journal articles on radio propagation and wireless system design. His main research interests are in the area of radio systems design and radio propagation channel theoretical modeling and experimental investigation. In April 1999, he was a recipient of the Marconi Foundation Young Scientist Prize in the context of the XXV Marconi International Fellowship Award.

Velio Tralli (Senior Member, IEEE) received the Dr.Ing. degree (cum laude) in electronic engineering and the Ph.D. degree in electronic engineering and computer science from the University of Bologna, Bologna, Italy, in 1989 and 1993, respectively.

From 1994 to 1999, he was a Researcher with the National Research Council, CSITE, University of Bologna. In 1999, he joined the Department of Engineering, University of Ferrara, Ferrara, Italy, where he is currently an Associate Professor. He has authored or coauthored more than 150 articles in refereed journals, including IEEE TRANSACTIONS and international conferences. He has participated in several national and European research projects addressing short-range communications systems, 3G/4G/5G wireless networks, wireless video communications, and on-chip optical wireless networks. His research interests include digital transmission and coding and wireless communications, with emphasis on radio resource optimization and cross-layer design. He served as the Co-Chair for the Wireless Communication Symposium of ICC 2006 and the Communication Theory Symposium of ICC 2013. He also serves as an Associate Editor for the *European Transactions on Emerging Technologies*.

Davide Bertozzi (Member, IEEE) received the bachelor's and Ph.D. degrees in electrical engineering from the University of Bologna, in 1999 and 2003, respectively. He is currently an Associate Professor at University of Ferrara (Italy), where he leads the MPSoC Research Group. The mission of his research is to stay at the forefront of system innovation by leveraging the enabling properties of communication architectures and emerging technologies. He has published around 180 scientific contributions in the field of interconnect-centric design and co-edited one book on networks-on-chip in 2010. He has worked in several research projects funded by the European Union (Galaxy, NaNoC, and vIrtical) and coordinated a pioneering national project on the applications of silicon photonics to computer communications (Photonica). He was a Visiting Researcher at international academic institutions (Stanford University) and semiconductor companies (STMicroelectronics, NXP, Samsung, and NEC). In 2018, he received the Wolfgang Mehr Award from the IHP Leibniz Institute for Innovative Microelectronics (Germany) for his research in the field of electro-optical interconnection fabrics for 3-D-stacked systems.

Giovanni Serafino received the Ph.D. degree (cum laude) in emerging digital technologies from the Sant'Anna School of Advanced Studies, Pisa, Italy, in 2013. He is a Project Manager at MBI Group, Pisa. He was an Assistant Professor at the Sant'Anna School of Advanced Studies. He is the coauthor of more than 30 articles on international journals and more than 70 papers on conference proceedings, two book chapters, and five patents. Among his past and actual research interests, there are all-optical signal processing, fiber-optic transmission systems, reconfigurable nodes for optical networks, applications of microwave photonics techniques to radar systems and wireless communications, including optical beamforming for 5G and photonics-assisted coherent MIMO radars.

Vincenzo Petruzzelli was born in Bari, Italy, in 1955. He graduated in electrical engineering from the University of Bari in 1986. He is currently engaged as an Associate Professor of electromagnetic at the Department of Electrical and Electronic Engineering, Polytechnic University of Bari. He is a member of Electronic Engineer Doctorate Courses. Over the years, he has dealt with various research topics, such as integrated plasmonic nanoantennas for wireless on-chip optical communications, innovative optical devices for the optical interconnects on chip, periodic structures for laser cavities based on the optical self-collimation property of mesoscopic structures, plasmonic periodic nanostructures for the realization of plasmonic sensors. He has coauthored over 330 publications, 132 of which published on international journals and 155 presented at international conferences. He was a member of the Management Committee of the MP0805 COST action "Novel Gain Materials and Devices Based on III-V-N Compounds." He acts as a Reviewer of European and National Projects.

Open Access funding provided by 'Università degli Studi di Ferrara' within the CRUI CARE Agreement